Green Chemistry

ROYAL SOCIETY OF CHEMISTRY

PAPER

View Article Online
View Journal | View Issue

Cite this: *Green Chem.*, 2024, **26**, 3229

Efficient removal of sulfonamides in complex aqueous environments by an N, P-co-doped graphitic biochar: the crucial role of P_2O_5†

Wei Tang, [a,b] Daniel S. Alessi, [c] Tongshuai Wang,[a,b,d] Jingqi Wu,[a,b] Shijia Li,[a,b] Kurt O. Konhauser,[c] Zhixiong Li[a,b] and Jiawei Chen *[a,b]

Received 2nd December 2023,
Accepted 22nd January 2024

DOI: 10.1039/d3gc04731h

rsc.li/greenchem

Sulfonamides (SAs) have long been utilized as synthetic antibiotics against bacterial and protozoan infections. Despite their efficacy, SAs can cause significant environmental toxicity, promoting the development of various elimination techniques. This study aimed to develop a biochar efficient at removing SAs from complex aqueous solutions and is the first to establish the role of P_2O_5 in advanced oxidation processes (AOPs). To do so, a range of biochars was developed. The best-performing biochar (NPBC900) can remove 98.33% of a 20 mg L^{-1} solution of sulfapyridine within 120 minutes using just 0.1 g L^{-1} of catalyst and 0.5 mM disulfate, surpassing AOP catalysts developed to date. Furthermore, solution components including inorganic anions and cations and natural organic matter have almost no effect on the sulfonamide elimination efficiency, which we demonstrated by testing several natural waters. In this system, it was observed that $^1O_2$ and electron transfer played the greatest roles in the overall oxidation process. The best biochar, NPBC900, exhibited exceptional stability and reusability, and the degradation byproducts including residual sulfapyridine did not show any noticeable phytotoxicity. This study presents a cost-effective solution for environmental sulfonamide remediation and underscores the vital role of P_2O_5 in AOPs.

1. Introduction

The presence of antibiotics in aqueous environments has garnered significant attention because their incomplete elimination and discharge from sewage treatment plants can lead to environmental contamination.[1] Furthermore, prolonged exposure of an environment to antibiotics may contribute to the emergence of bacterial resistance, sometimes leading to the reproduction of superbugs and super-viruses and potentially triggering a global pandemic.[2] Sulfapyridine (SPY) is one of the most commonly used sulfonamide antibiotics (SAs), primarily employed as a veterinary drug for prophylactic or therapeutic purposes in animal husbandry. SPY is frequently detected in aqueous environments;[3] for example, 0.51 μg L^{-1} of SPY was found in river water in Hong Kong,[4] while concentrations as high as 19.2 μg L^{-1} were found in surface water and groundwater in many countries, including Korea, China, and the USA.[5] Numerous studies have demonstrated that SPY has harmful effects on aquatic life and humans, including biological toxicity, endocrine disruption, and carcinogenicity.[6] As a result, various techniques have been developed to eliminate SPY from aquatic environments.

Adsorption technologies for carbon-based materials, such as carbon nanotubes, activated carbon, biochar, *etc.*, have received recent attention for the removal of antibiotics from aqueous solutions due to their low cost, simplicity of implementation, and absence of secondary pollution.[7] However, adsorption processes are inherently limited in their ability to decompose antibiotics, and in many cases, there is a real risk of antibiotic desorption back into water. As a consequence, focus has been placed on pre-adsorption processes that can enhance subsequent degradation during the removal of antibiotics.[8] In this regard, persulfate-based advanced oxidation processes (PS-AOPs) are regarded as a promising technology for antibiotic degradation due to their ability to operate effectively over a wide pH range (3 to 9), their powerful oxidizing capacity ($SO_4^{\bullet-}$ = 2.8 to 3.1 V), and the substantial duration of their active oxygen life which is a measure of 40 μs

[a]*State Key Laboratory of Biogeology and Environmental Geology, China University of Geosciences, Beijing 100083, P. R. China*
[b]*School of Earth Sciences and Resources, China University of Geosciences, Beijing 100083, P. R. China. E-mail: chenjiawei@cugb.edu.cn; Tel: +86-10-82321959*
[c]*Department of Earth and Atmospheric Sciences, University of Alberta, Edmonton, Alberta T6G 2E3, Canada*
[d]*China Household Electric Appliance Research Institute (CHEARI), Beijing 100053, P. R. China*

†Electronic supplementary information (ESI) available. See DOI: https://doi.org/10.1039/d3gc04731h

(>$^{\bullet}$OH = 1 μs).[9,10] Nonetheless, PS-AOPs may be vulnerable to interference and self-quenching by environmental substances during the free radical-mediated contaminant degradation pathways.[11] Therefore, non-radical pathways based on singlet oxygen ($^1O_2$) and direct electron transfer have garnered particular attention as they may perform more effectively in complex aquatic environments.[12] The primary persulfates used include monosulfate (PMS, HSO_5^-) and disulfate (PDS, $S_2O_8^{2-}$). PDS is more challenging to activate than PMS, but it is more stable, less expensive, and easier to transport.[13] Moreover, combining adsorption technologies and PDS-AOPs can result in synergies that can achieve more effective and thorough elimination of antibiotic sulfonamides from aquatic environments.

Biochar is regarded as an economic adsorbent for the removal of various pollutants from soil and water. The modification of biochar through nitrogen doping can significantly improve its adsorption capacity for certain contaminants such as SAs, as well as enhance its catalytic effect.[14,15] Zhu *et al.* prepared nitrogen-doped graphitic biochar and distinguished the roles of adsorption and catalytic performance in non-radical PDS activation,[8] while Wan *et al.* elucidated the crucial role of the nitrogen form and nitrogen vacancies in non-radical pathways.[16] Recently, Deng *et al.* identified phosphorus as a critical component in the formation of $^1O_2$,[17] and Li *et al.* showed that the N–P co-doping strategy has a synergistic effect on enhancing the catalytic activity of biochar.[18]

Despite these advances, critical information about the speciation of P in N–P co-doped biochars and the mechanisms of its involvement in AOPs remains unresolved. Furthermore, synthesizing N–P co-doped biochars in a straightforward manner while ensuring the efficient removal of antibiotics in complex aquatic environments remains a challenge. Therefore, to obtain an optimized modified biochar, here we propose a simple one-step pyrolysis method as a surface doping process. We utilized environmentally friendly ammonium polyphosphate (APP) as the precursor source of N and P. The arrangement of N and P species was controlled by adjusting the pyrolysis temperature and the biomass-to-APP doping ratio, with the final speciation confirmed by various analytical methods, including FTIR, XPS, XRD, and Raman spectroscopy. This study not only offers a cost-effective solution for the environmental remediation of sulfonamides but also sheds light on the importance of P speciation in N–P co-doped biochars for AOPs.

2. Materials and methods

2.1 Materials

All chemicals used in this study were of analytical reagent grade or higher and used without further purification. More information can be found in the ESI (Text S1†).

2.2 Preparation of biochar

A procedure similar to that of Tang *et al.* was used to synthesize N/P-doped biochar (NPBC).[14] The detailed process with some modifications is provided in Fig. S1† and discussed in detail in the ESI (Text S2†). Several common catalysts were synthesized for comparison, including Fe_3O_4, Mn_2O_3, Fe_2O_3, H_3PO_4@BC900, KOH@BC900, NBC900, Fe@BC900, Fe@NBC900 and ONPBC900.[14,19–22] Detailed source and abbreviation definitions are provided in Text S2.†

2.3 Characterization of biochar

The characterization methods are provided in the ESI (Text S3†). NPBC samples were characterized using Raman spectroscopy (Renishaw Raman spectrometer, UK), scanning electron microscopy with an energy dispersive X-ray spectrometer (SEM-EDS; Zeiss Supra 55-VP, Germany), Fourier transform infrared (FTIR) spectroscopy (Nicolet iS10 spectrometer, Thermo Fisher Scientific, Massachusetts, USA) and X-ray photoelectron spectroscopy (XPS; ESCALAB 250Xi Thermo Fisher Scientific, Massachusetts, USA). Electron spin resonance (EPR; Bruker, Germany) analysis was performed using spin-trapping agents DMPO and TEMP; specific experimental conditions are provided in the ESI (Text S4†). An electrochemical method was also employed to detect the electron transfer process during degradation (Text S5†).[19]

2.4 Batch experiments and analytical methods

Batch adsorption experiments were carried out at room temperature (25 °C ± 2 °C). The adsorption rates and capacities were calculated using adsorption kinetics and equilibrium adsorption isotherm models, respectively (Text S6†). The catalytic performance of NPBC was evaluated at room temperature (25 °C ± 2 °C) in a batch reactor containing 200 mL of aqueous solution. Briefly, 2 mL of 2 g L^{-1} SPY stock solution was mixed with 20 mL of 0.1 M $NaNO_3$ and diluted to 200 mL with DI water in a bottle without pH adjustment (pH = 6.71 ± 0.10). Next, 20 mg of NPBC (particle size < 0.5 mm) was added to the bottle. Pre-adsorption was conducted for 10 min to uniformly disperse the biochar particles. Then, 1.25 mL of PDS (20 mM) was added to the bottle. Catalytic degradation experiments were conducted with 0.1 g L^{-1} catalyst and 0.5 mM PDS. At certain pre-determined time intervals, 0.6 mL of solution was collected and filtered through a 0.22 μm polyethersulfone (PES) membrane into a brown glass vial and 0.6 mL of ethanol was added to the vial to quench the oxidation during the preparation for analysis by high-performance liquid chromatography (HPLC). The impacts of the doping ratio and pyrolysis temperature of the catalyst were comparatively assessed. The common metal and metal-free catalysts (Fe_3O_4, Mn_2O_3, Fe_2O_3, H_3PO_4@BC900, KOH@BC900, NBC900, Fe@BC900, Fe@NBC900 and ONBC900) were also evaluated for PDS activation.

The concentrations of SPY and other sulfonamides were analyzed using a HPLC (LC-20AD, Shimadzu, Kyoto, Japan). The oxidation intermediates were identified using a LC-mass spectrometer (ESI-MS, Triple Quad 3500, AB Sciex, USA). The mineralization of SPY was determined using a total organic carbon analyzer (TOC-V WP, Shimadzu, Kyoto, Japan). Details of the analytical methods are provided in ESI Texts S7 and S8.†

Various quenching agents (methanol, *p*-benzoquinone, *tert*-butanol, furfuryl alcohol, L-histidine and KI) were used to identify the radical species in the NPBC/PDS system. Environmental factors in an aqueous solution including anions, coexisting heavy metals, natural organic matter, and the use of field-collected water samples were investigated in order to properly consider the performance of materials in complex aquatic environments. Finally, phytotoxicity assay experiments were conducted to assess the overall safety of antibiotic adsorption and degradation processes (Text S9†).

3. Results and discussion

3.1 Preparation and optimization of NPBC

To obtain an optimal biochar for the removal of SAs, a series of NPBCs were synthesized with different doping ratios of biomass and APP and at different temperatures. As a first set, biochars with varying doping ratios were synthesized at 900 °C. As shown in Fig. 1a and S2,† NPBC900 (2 : 1.1) exhibited the highest SPY removal efficiency (K_{obs} = 0.0342 min^{-1}). Under the conditions of initial SPY = 20 mg L^{-1}, PDS = 0.5 mM and biochar = 0.1 g L^{-1}, 98.3% of SPY was removed within 120 min. Specifically, when the APP doping ratio was increased from 1 : 0 to 2 : 1.1, the observed rate of SPY removal increased from 0.0017 min^{-1} to 0.0342 min^{-1}, while it decreased from 0.0342 min^{-1} to 0.0082 min^{-1} when further APP was added (from 2 : 1.1 to 1 : 5).

As indicated in Fig. 1a and b, NPBC900-1 : 5 contains the highest N and P contents; however, the SPY removal efficiency was not the highest with this material. This is because the speciation of heteroatoms plays a crucial role in AOPs rather than their total content.[20] For further illustration, FTIR, XPS, XRD, and Raman analyses were performed (Fig. 1b and d, S3–S7 and Table S1†), with specifics of the analyses described in Text S10.† An increase in surface-bound reactive species and higher graphitization of the NPBC900 (2 : 1.1) surface are responsible for the efficient removal of SPY, according to these analyses.

Secondly, a series of NPBCs were prepared at 300–900 °C using a doping ratio of 2 : 1.1 of biomass and APP. As shown in Fig. 1c and Fig. S8, S9,† NPBC900 had the highest SPY removal efficiency (K_{obs} = 0.0342 min^{-1}), which was found to be 16 to 43 times faster than other biochars (K_{obs} = 0.0008 to 0.0021 min^{-1}). The removal of SPY increased significantly with the NPBC pyrolysis temperature. We attribute this to the increased P_2O_5 content with temperature over much of the tested temperature range (Fig. S10†), which leads to the generation of more $^1O_2$. However, when the temperature is too high, the activity of the sample dramatically decreases (K_{obs} near 0 min^{-1}) due to the near complete loss of N and P dopants, as well as the collapse of the carbon framework (Fig. S8, S9 and Table S2†). Correlation analysis ($p < 0.01$) between P_2O_5 and C_t/C_0 was also performed (Fig. 2), and the positive correlation indicates that the P_2O_5 content is critical. Considering that P atoms play an important role in the formation of $^1O_2$,[4] and can directly contribute to the removal of SPY, we hypothesize that P_2O_5 plays a key role in AOPs.

FTIR, XPS, XRD, and Raman analyses were used to validate these mechanisms (Fig. S3, S10, S11 and Table S2†), with specifics of the analyses given in Text S11.† These results suggest that the reason for the superior performance of NPBC900 in removing SPY is its high density of surface-active complexes, as well as its strong electron-transfer ability as a consequence of the high degree of graphitization and the high degree of defects. Overall, NPBC900 (2 : 1.1) is the optimal biochar and, therefore, we studied it further in subsequent experiments.

3.2 Physicochemical properties of NPBC900

The SEM images in Fig. S12a† show that the pristine biochar has a characteristic honeycomb structure with a well-developed pore network. After N and P co-doping, NPBC900 displayed a distinctly different morphology, featuring increased macroscopic porosity and a smoother surface (Fig. S12b and c†). As evident in the elemental mapping images, the distribution of N and P could be clearly observed, confirming the successful doping of N and P (Fig. S12d and g†).

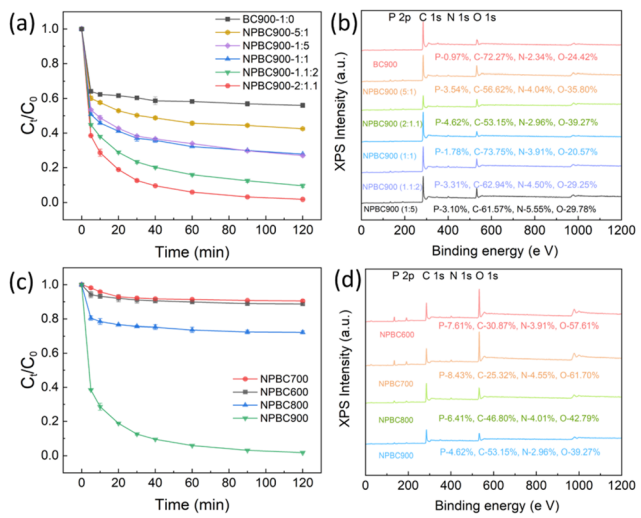

Fig. 1 PDS activation for SPY removal by NPBC synthesized with varying mass ratios of biomass and APP (a), XPS spectra (b), PDS activation for SPY removal by NPBC synthesized at high pyrolysis temperatures (c), XPS spectra (d) (reaction conditions: SPY = 20 mg L^{-1}, PDS = 0.5 mM, catalyst = 0.1 g L^{-1}, initial solution pH = 6.71).

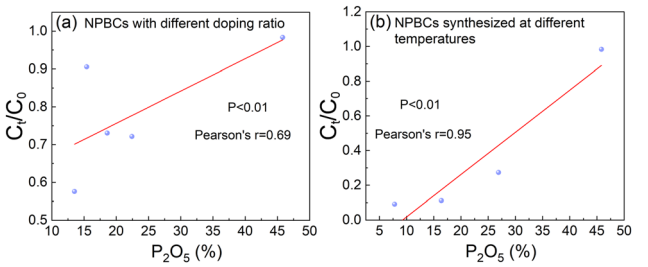

Fig. 2 The correlation analysis between P_2O_5 and the C_t/C_0 ratio on NPBCs.

The changes in the elemental composition of biochar, before and after N and P doping, were quantified using an elemental analyzer (Table S3†). The addition of APP as the N and P source reagent for producing NPBC900 resulted in an increase in the total N content from 1.61 wt% to 1.95 wt%, indicating the successful introduction of N. The H/C and (O + N)/C ratios, as well as the indices of aromaticity and hydrophilicity,[21] changed in NPBC900 as compared to the pristine biochar, indicating a decrease in aromaticity and an increase in hydrophilicity. These changes are consistent with a stronger H-bonding effect during SPY adsorption on NPNC900 which led to accelerated SPY removal from the aqueous solution.

3.3 The removal performance of NPBC900

The adsorption of organic compounds on the catalyst surface is generally considered the first step of heterogeneous catalytic degradation.[22] The adsorption performance of NPBC900 and BC900 towards SPY was systematically studied by classical adsorption kinetics and thermodynamics experiments (Fig. S13a, b and Tables S4, S5†). The details of the experimental analyses are provided in Text S12.† The results show that the adsorption of SPY on NPBC900 can be attributed to a chemical monolayer adsorption dominated by the surface-bound reactive species, such as hydroxyl groups (–OH), carbonyl groups (–C═O), and carboxyl groups (–COOH). These functional groups can interact with SPY through hydrogen bonding, acid–base reactions, and other interactions, thereby facilitating the adsorption process. NPBC900 possesses a significantly higher meso-porous volume than BC900 (Fig. S13c, d and Table S6†), indicating that it can promote rapid diffusion kinetics and enhance contact with organic pollutants or oxidants in solution.

The activation performance of NPBC900 was systematically studied by evaluating its ability to remove SPY. As depicted in Fig. 3a and S14,† when only PDS was used, the removal of SPY was negligible (K_{obs} near 0 min^{-1}). However, when BC900 was added, 44.01% of SPY was removed by BC900 and PDS (K_{obs} = 0.0017 min^{-1}), which was lower than the SPY removal efficiency of BC900 alone (52.8%, K_{obs} = 0.0060 min^{-1}). This result is likely due to the low V_{meso} value of BC900 (0.105 cm^3 g^{-1}) which is not conducive to the fast diffusion kinetics and contact of the BC900 surface with SPY or PDS (Table S6†). In addition, the pores might have become further clogged after PDS was added, leading to a decrease in the SPY removal efficiency. With the introduction of N and P, the removal rate of SPY increased from 52.8% to 58.33% for NPBC900. Interestingly, the simultaneous addition of PDS and NPBC900 resulted in a significant enhancement in the SPY removal efficiency. Together, they led to 98.33% of SPY being removed within 120 min. The K_{obs} value of NPBC900 + PDS (0.0342 min^{-1}) was 20.12 times higher than that of BC900 + PDS (0.0017 min^{-1}), indicating significantly improved catalytic activity. This improvement is stronger than most reported catalysts in AOPs (Table S7†).

The enhanced activation performance of NPBC900 + PDS could be attributed to the synergistic effect of N and P co-doping,[18] which is not unexpected given that N and P co-doping provides more active sites and further adjusts the local charge density of the carbon network to promote further electron transfer. The XRD and Raman spectra of NPBC900, collected before and after its use, confirm this (Fig. 3b and c).

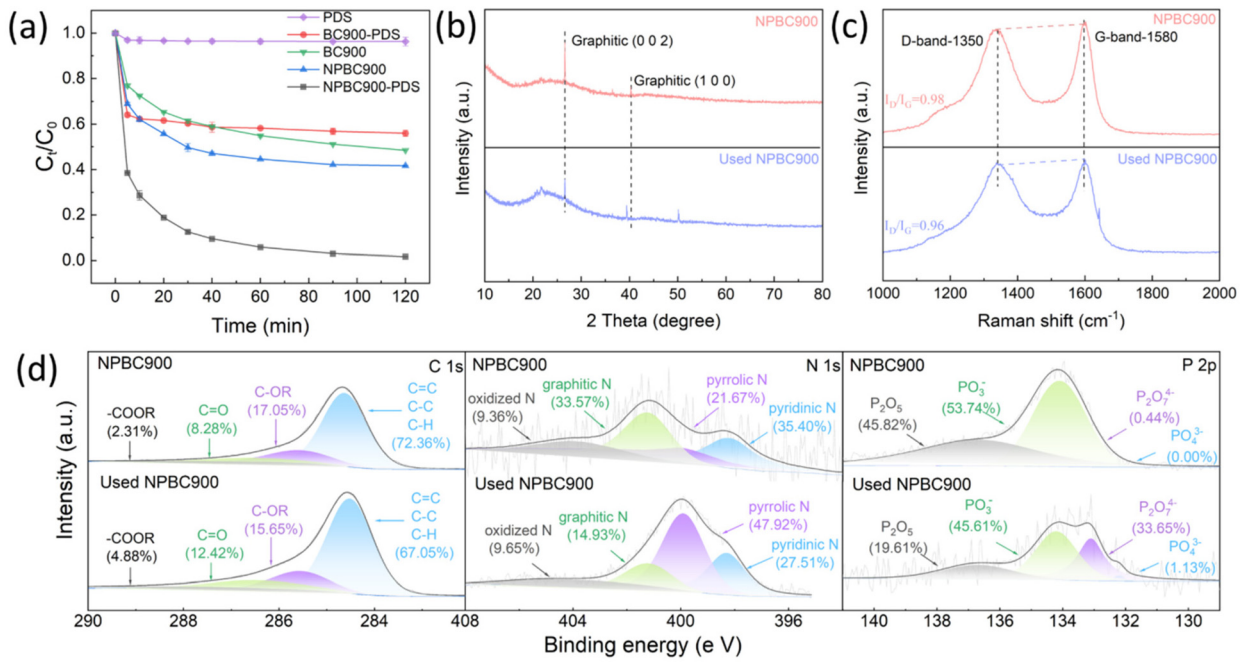

Fig. 3 SPY removal performance (a); XRD (b), Raman (c) and XPS spectra of NPBC900 and used NPBC900 (d).

The reduction of (002) and (100) peaks, as well as ID/IG values, in the used NPBC900 indicate the loss of graphite and structural defects. This results in a decrease in the surface active sites and electron transfer capacity, suggesting that the active sites and electron transfer mechanisms are involved in the SPY removal process. The decrease in the graphitic N content observed in Fig. 3d, from 33.57% to 14.93%, also supports this argument. Moreover, the sharp decrease in the P 2p/C 1s ratio, from 0.09 to 0.01, particularly in the P_2O_5 content from 45.82% to 19.61%, suggests the crucial role of singlet oxygen ($^1O_2$) in SPY removal (Table S8†). The content of C-OR on NPBC900 also decreased from 17.05% to 15.65% after SPY was used, confirming the role of the H-bonding effect and implying that adsorption is involved in the removal of SPY in the NPBC/PDS system.

In addition, a series of desorption experiments were performed to determine the stability of SPY on the NPBC surface. Fig. S15a† shows that NPBC900 + PDS + SPY had the highest SPY removal efficiency (98.63%), and almost no SPY was found after the desorption step (0.83%). In contrast, NPBC900 + SPY not only had low SPY removal efficiency (63.65%) but also showed a substantial amount of SPY in solution after desorption (44.12%). This means that using NPBC + PDS + SPY, a reliable and robust SPY removal process is achieved. Meanwhile, PDS depletion in Fig. S15b† is positively correlated with SPY removal, proving that this process is a degradation-dominated process. Furthermore, in the SEM-EDS images of NPBC900, before and after use (Fig. S16†), we observed that the N and P on the surface of NPBC900 were not easily lost, which means that the use of NPBC900 in water is safe and sustainable.

3.4 Optimization of experimental parameters for SPY removal

While our results clearly show that NPBC900 has the highest SPY removal efficiency, we conducted a series of experiments with varying parameters such as pH, PDS dosing, NPBC900 dosing, and SPY concentration, including a variety of comparative catalyst experiments for AOPs, to verify the accuracy of the experimental parameters and the superiority of NPBC (Fig. S17 and Fig. S18†). These analyses are documented in Text S13† in detail.

High SPY removal rates (95.54%–98.39%) were obtained over a broad pH range (pH 3–9), showing remarkable adaptability for water treatment (Fig. S17a†). However, the SPY elimination efficacy decreased at a more alkaline pH of 11 due to the inhibition of PDS activation. The electrostatic repulsion between the negatively charged NPBC900/SPY anionic/$S_2O_8^{2-}$ ternary systems was discovered at pH 11 by zeta potential analysis, resulting in decreased SPY removal efficiency (Fig. S17b†). Excess PDS concentrations also caused mutual quenching of reactive species; hence, an optimal PDS dosage of 0.5 mM resulted in almost complete SPY elimination (Fig. S17c†). The removal effectiveness of SPY decreased with increasing initial SPY concentration, which was attributable to the blocking of active sites and a lack of reactive oxygen species (ROS) (Fig. S17d†). The NPBC900 dose was linked positively with SPY removal, with 0.1 g L^{-1} catalyst achieving 96.98% SPY removal in 120 minutes (Fig. S17e†). When compared to other catalysts, NPBC900 showed the highest SPY elimination capability due to successful N and P element insertion and its graphitic structure that contained active sites (Fig. S17f†).

3.5 Effect of environmental factors on SPY removal

The effects of cations, anions, and humic acids on SPY removal were explored in order to replicate constituents found in natural waters and understand their impacts on SPY removal by the NPBC900/PDS system. These chemicals are ubiquitous in water and can interfere with catalytic oxidation by quenching ROS or competing for active sites.[23]

Cu(II) and Cr(VI) at a concentration of 20 mg L^{-1} were observed to slightly impair the removal effectiveness of SPY using the NPBC900/PDS system (Fig. 4a and S19a†). Over a duration of 120 minutes, the removal rate dropped from 98.33% to 92.72% and 89.62%, and the corresponding k_{obs} value dropped from 0.0342 min^{-1} to 0.0158 and 0.0153 min^{-1}. This is because when NPBC900 was used, Cu(II) and Cr(VI) were adsorbed on the surface of NPBC900, reducing the number of active sites available (Fig. S20†). In addition, NPBC has the ability to convert soluble Cr(VI) into relatively insoluble Cr(III) *via* a reduction process. However, the formation of the resulting Cr(III) hydroxide precipitates limits the activation potential of the catalyst even further by partially coating the surface of NPBC.[14] Similarly, 0.2 g L^{-1} HA hindered the elimination of SPY to some extent (87.01%, 0.0111 min^{-1}). This could be related to the adsorption of HA on the surface of NPBC900 which contains carboxyl and phenolic hydroxyl groups. This can interfere with the interaction of the active site of NPBC900 with PDS, decreasing the oxidation reaction.[22] Nonetheless, in all cases the removal efficiency of SPY remains relatively high.

For some common anions, such as Cl^-, $H_2PO_4^-$, SO_4^{2-}, and HCO_3^-, there was essentially no influence on the elimination of SPY (ionic strength: 10 mM; 96.07–98.41% removal and 0.0179 to 0.0307 min^{-1}), as shown in Fig. 4b and S19b.† This suggests that the majority of anions have no impact on SPY removal in the NPBC/PDS system. Conversely, a significant inhibitory effect was found after the addition of 10 mM CO_3^{2-} (64.95% removal and 0.0071 min^{-1}). The inhibitory effect of CO_3^{2-} may be due to the consumption of superoxide radicals ($O_2^{\bullet-}$) (eqn (1) and (2), where $O_2^{\bullet-}$ may react with water or self-recombine to form $^1O_2$ (eqn (3) and (4)), resulting in a reduction of $^1O_2$.

$$CO_3^{2-} + O_2^{\bullet-} \rightarrow {}^{\bullet}CO_3^{-} + O_2^{2-} \quad (1)$$

$${}^{\bullet}CO_3^{-} + O_2^{\bullet-} \rightarrow {}^{\bullet}CO_3^{2-} + O_2 \quad (2)$$

Additional experiments were carried out in a 10 mM $NaNO_3$ solution (control), tap water, and river water to further test the use of the NPBC900/PDS system in natural water. The removal efficiency of SPY in tap and river water was slightly lower when compared to the control (Fig. 4c); removal rates of 94.17% and

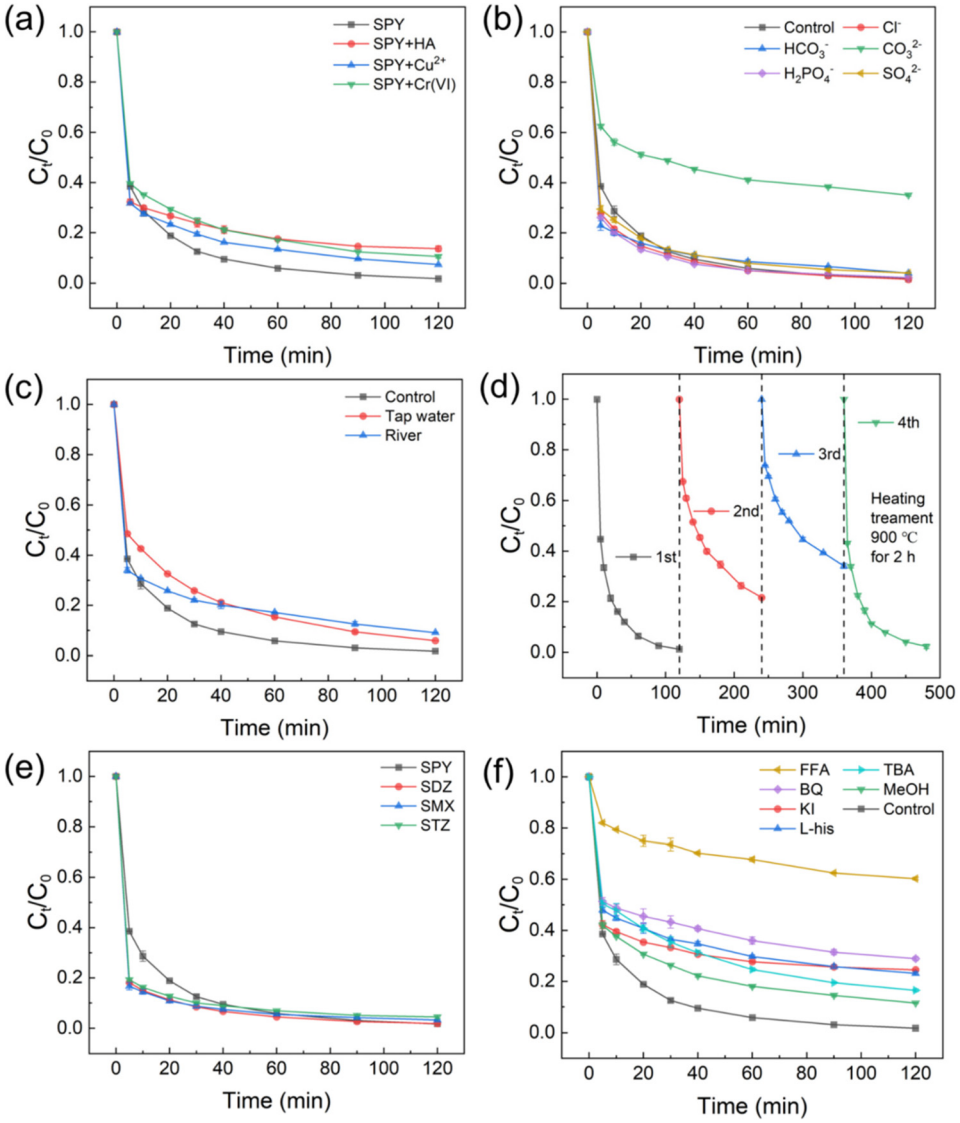

Fig. 4 Influence of inorganic anions and humic acids on SPY removal (a and b); effect of a natural water matrix on SPY removal (c); repeated SPY removal and NPBC900 recovery (d); removal of other sulfonamides (e); effects of radical inhibitor on SPY removal (f).

90.90% were observed, with the corresponding k_{obs} values of 0.0211 min^{-1} and 0.0125 min^{-1}, respectively (Fig. S19c†). Overall, despite the presence of various types of organic or inorganic compounds in the waters, NPBC900/PDS was found to be highly effective in removing SPY from complex aqueous environments.

In practical applications, the stability of catalysts is a crucial aspect that must be considered. Therefore, the reusability of NPBC900 was evaluated by performing four consecutive recovery tests (Fig. 4d). The results showed that the removal efficiency decreased to 78.39% and 65.92% in the 2nd and 3rd runs, respectively. The observed decrease in the activity of NPBC900 after multiple recoveries could be attributed to the accumulation of intermediates on the surface which hindered the interaction between PDS and active sites, as well as changes in surface chemistry and electron conductivity. The FTIR spectra of NPBC900, before and after use, exhibited a shift in the C=C vibration band and an increase in intensity (Fig. S11†). This suggests that some organic compounds were adsorbed onto the surface of NPBC900. Yet, when NPBC900, which had been used multiple times, was pyrolyzed at 900 °C under a N_2 flow for 2 h, its catalytic activity was essentially restored. The removal rate of SPY in the 4th recovery run was 97.73%, which was almost the same as the first use effect (98.81%). This phenomenon can be attributed to the decomposition of the intermediates during pyrolysis which leads to the exposure of active sites.

NPBC900/PDS also demonstrated an excellent removal capacity for the most common sulfonamide antibiotics, such as sulfadiazine (SDZ), sulfamethoxazole (SMX), and sulfathiazole (STZ). As shown in Fig. 4e and S19d,† 98.18%, 96.78% and 95.58% removal rates were observed at SDZ, SMX and

STZ, with the corresponding k_{obs} values of 0.0244 min^{-1}, 0.0189 $min^{-1}$and 0.0169 min^{-1}, respectively. The results of the standard line test for the four SAs provide evidence of the reliability of these findings (Fig. S21,† $R^2 > 0.999$).

Quenching experiments with several scavengers were carried out to better understand the primary active species (*e.g.*, $^{\bullet}OH$, $SO_4^{\bullet-}$, and $^1O_2$) in the NPBC900/PDS system, as documented in Text S14† in detail. The results show that $-^{\bullet}OH$ plays a greater role in the removal of SPY than $SO_4^{\bullet-}$ in the reaction. This is confirmed by the inhibitory effect found when 500 mM TBA/PDS and 500 mM MeOH/PDS were introduced, with TBA/PDS exerting a greater constraint. Additionally, given their position as common quenchers of $^1O_2$, the strong inhibitory effect of 100 mM furfuryl alcohol (FFA) and 10 mM L-histidine (L-His) suggests that singlet oxygen ($^1O_2$) is the predominant active species responsible for SPY elimination. Furthermore, the presence of *p*-benzoquinone (BQ), a typical superoxide radical ($O_2^{\bullet-}$) scavenger, and the efficiency of 10 mM KI in blocking SPY removal demonstrate the involvement of $O_2^{\bullet-}$and surface-bound reactive species in the NPBC900/PDS system.

3.6 Identification of ROS and the mechanism

To further identify reactive oxygen species (ROS), electron spin resonance (EPR) spectroscopy was conducted. DMPO was used as a spin-trapping agent for $^{\bullet}OH$ and $SO_4^{\bullet-}$ (Fig. 5a). A clear EPR signal was not detected in either the DMPO or DMPO + PDS system, indicating that PDS cannot be activated by itself. However, after adding NPBC900, the characteristic signal of DMPO oxidation by $^{\bullet}OH$ and $SO_4^{\bullet-}$ (DMPOX) was observed and strengthened over time. Based on the quenching experiment results, the contents of $^{\bullet}OH$ and $SO_4^{\bullet-}$ radicals were found to be low. DMPO can also be oxidized by $^1O_2$ with a rate constant of about 1.8 × 107 M^{-1} s^{-1};[24] thus, it was assumed that the DMPOX measured was produced from DMPO oxidation by $^1O_2$. To confirm the $^1O_2$ species, TEMP was added to the reaction system as a $^1O_2$ spin trap. As shown in Fig. 5b, TEMP alone and TEMP + PDS did not result in an EPR signal, but upon addition of NPBC900, a clear TEMP-$^1O_2$ signal appeared, indicating the presence of $^1O_2$. Furthermore, the TEMP-$^1O_2$ signal increased from 30 min to 60 min and persisted for up to 120 min, indicating a continuous production of $^1O_2$. In summary, $^1O_2$ played a major role in the removal of SPY.

In addition to $^1O_2$, direct electron transfer is another non-radical pathway that can facilitate the removal of organic pollutants in carbon-activated persulfate systems.[19] Cyclic voltammetry and current–time curves were employed to investigate whether NPBC900 mediated electron transfer from SPY to PDS. Electrochemical (EC) oxidation currents were measured in three distinct systems: NPBC900 only, NPBC900 with PS, and NPBC900 with PDS/SPY. It is apparent that NPBC900

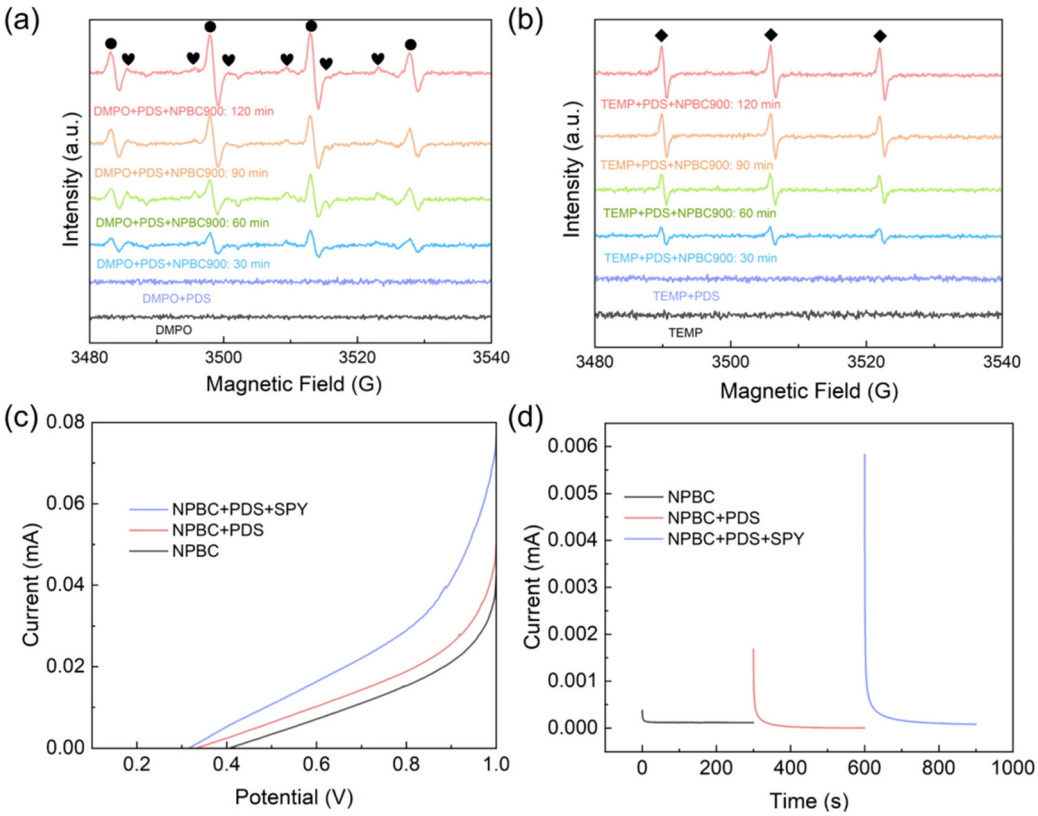

Fig. 5 The EPR spectra with the addition of DMPO (a) and TEMP (b) at different reaction times; cyclic voltammetry (c) and current–time curves (d) of NPBC900.

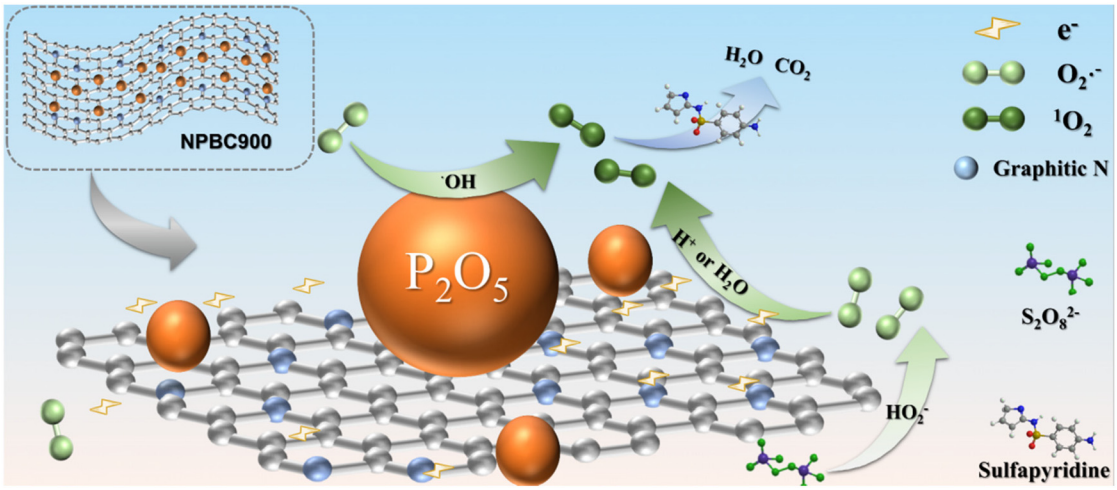

Fig. 6 Proposed SPY removal mechanisms in the NPBC900/PDS system.

alone had no apparent EC activity (Fig. 5d and e), but upon addition of PDS and SPY, noticeable EC activity was observed. This suggests the possible involvement of a direct electron transfer process in the NPBC900/PDS/SPY system.

Considering the above analysis, a proposed removal mechanism is shown in Fig. 6. Initially, the kinetics of SPY and $S_2O_8^{2-}$ removal from solution by NPBC900 surfaces was rapid due to diffusion into mesopores. Once adsorbed, the graphitic and defect-containing structure of NPBC900 can act as a bridge to transfer electrons to electrophilic PDS and initiate the reaction of $S_2O_8^{2-}$ with H_2O or self-recombination to HO_2^- (eqn (5)). The subsequent formation of $O_2^{\bullet-}$ and $^{\bullet}OH$ was attributed to the reaction of $S_2O_8^{2-}$ with HO_2^- (eqn (6) and (7)). Meanwhile, the $O_2^{\bullet-}$ generated can be used as a precursor to form $^1O_2$ in three ways: (1) $O_2^{\bullet-}$ combines with H^+ (eqn (3)) or H_2O (eqn (4)) to form $^1O_2$; (2) $O_2^{\bullet-}$ combines with OH, $SO_4^{\bullet-}$ and/or P_2O_5 to form $^1O_2$ (eqn (8)–(10)); and (3) self-recombination of $O_2^{\bullet-}$ can produce $^1O_2$.[22] In addition, some of the $^1O_2$ might be involved in the activation of PDS due to the structural defects in NPBC900. Overall, $O_2^{\bullet-}$, $^1O_2$, $^{\bullet}OH$ and $SO_4^{\bullet-}$ all contributed to SPY removal, with $^1O_2$ playing a major role and $^{\bullet}OH$ and $SO_4^{\bullet-}$ playing a secondary role. In combination with P_2O_5, $O_2^{\bullet-}$ acts as a precursor for the production of $^1O_2$ rather than oxidizing SPY directly.

$$2O_2^{\bullet-} + 2H^+ \rightarrow {}^1O_2 + H_2O_2 \quad (3)$$

$$2H_2O + 2O_2^{\bullet-} \rightarrow {}^1O_2 + 2OH^- + H_2O_2 \quad (4)$$

$$S_2O_8^{2-} + 2H_2O \rightarrow HO_2^- + 2SO_4^{2-} + 3H^+ \quad (5)$$

$$S_2O_8^{2-} + HO_2^- \rightarrow SO_4^{2-} + SO_4^{\bullet-} + O_2^{\bullet-} + H^+ \quad (6)$$

$$SO_4^{\bullet-} + OH^- \rightarrow {}^{\bullet}OH + SO_4^{2-} \quad (7)$$

$$O_2^{\bullet-} + {}^{\bullet}OH \rightarrow {}^1O_2 + OH^- \quad (8)$$

$$O_2^{\bullet-} + SO_4^{\bullet-} \rightarrow {}^1O_2 + SO_4^{2-} \quad (9)$$

$$P_2O_5 + 4O_2^{\bullet-} \rightarrow P_2O_7^{4-} + 3\,{}^1O_2 \quad (10)$$

3.7 SPY degradation pathways and intermediate toxicity

ESI-MS analysis was employed to identify the degradation intermediates of SPY and infer about their molecular structures based on the measured *m*/*z* values and by comparison with previous relevant research (Fig. S22 and S23†). Possible degradation pathways are proposed (Fig. S24†) and documented in Text S15† in detail. Briefly, SPY degradation occurs *via* a set of reactions in which active species target particular bonds, resulting in the generation of several intermediate products (P1–P14). These intermediates undergo further transformations, such as cleavage, extrusion, and substitution processes, resulting in the creation of smaller molecules, the majority of which are oxidized to CO_2 and H_2O. This was demonstrated in our systems by significant TOC removal (70%) and the elimination of the SPY signal in the chromatography over time (Fig. S25†). In addition, a phytotoxicity test (Fig. S26†) was performed to assess the toxicity of the breakdown products, details of which can be found in the ESI (Text S16†). These results indicated that the NPBC900/PDS system successfully removed the phytotoxicity of SPY and its breakdown intermediates, and even stimulated plant development due to a small but effective amount of N and P leaching.

4. Conclusions and environmental implications

We successfully synthesized a suitable biochar to remove sulfonamides from complicated aquatic environments. Our work is also the first to establish the role of P_2O_5 in AOPs. In this mechanism, $^1O_2$ and electron transfer played critical roles in

the elimination of SPY. The developed biochar efficiently removes 98.33% of 20 mg L^{-1} sulfapyridine in 120 minutes using only 0.1 g L^{-1} of catalyst and 0.5 mM PDS, outperforming the prevailing AOP catalysts. Furthermore, the elimination effect was essentially unaffected by external factors such as anions and cations, and natural organic matter in solution. It was also exceptionally stable, reusable, and safe. Based on the investigation of intermediates measured by ESI-MS, this work presented five probable degradation pathways and demonstrated that SPY breakdown byproducts have no substantial phytotoxicity. Overall, the cost-effective and environmentally friendly NPBC/PDS system we developed offers a promising alternative for long-term and practical water remediation.

Conflicts of interest

All of the authors declared no conflict of interest.

Acknowledgements

This work was supported by the National Natural Science Foundation of China (41731282) and the Fundamental Research Funds for the Central Universities (2652021104).

References

1 J. Wang, M. Yue, Y. Han, X. Xu, Q. Yue and S. Xu, Highly-efficient degradation of triclosan attributed to peroxymonosulfate activation by heterogeneous catalyst g-C_3N_4/$MnFe_2O_4$, *Chem. Eng. J.*, 2020, **391**, 123554.

2 J. He, T. Xie, T. Luo, Q. Xu, F. Ye, J. An, *et al.*, Enhanced peroxymonosulfate activation over heterogeneous catalyst Cu $_{0.76}$ Co $_{2.24}$ O $_4$/SBA-15 for efficient degradation of sulfapyridine antibiotic, *Ecotoxicol. Environ. Saf.*, 2021, **216**, 112189.

3 V. Moreno, A. Adnane, R. Salghi, M. Zougagh, O. S. Iacute, *et al.*, Nanostructured hybrid surface enhancement Raman scattering substrate for the rapid determination of sulfapyridine in milk samples, *Talanta*, 2019, **194**, 357–362.

4 W. Deng, N. Li, H. Zheng and H. Lin, Occurrence and risk assessment of antibiotics in river water in Hong Kong, *Ecotoxicol. Environ. Saf.*, 2016, **125**, 121–127.

5 W. Baran, E. Adamek, J. Ziemiańska and A. Sobczak, Effects of the presence of sulfonamides in the environment and their influence on human health, *J. Hazard. Mater.*, 2011, **196**, 1–15.

6 J. Huang, A. R. Zimmerman, H. Chen and B. Gao, Ball milled biochar effectively removes sulfamethoxazole and sulfapyridine antibiotics from water and wastewater, *Environ. Pollut.*, 2020, **258**, 113809.

7 S. Yanan, X. Xing, Q. Yue, B. Gao and Y. Li, Nitrogen-doped carbon nanotubes encapsulating Fe/Zn nanoparticles as a persulfate activator for sulfamethoxazole degradation: role of encapsulated bimetallic nanoparticles and nonradical reaction, *Environ. Sci.: Nano*, 2020, **7**(5), 1444–1453.

8 S. Zhu, X. Huang, F. Ma, L. Wang, X. Duan and S. Wang, Catalytic Removal of Aqueous Contaminants on N-Doped Graphitic Biochars: Inherent Roles of Adsorption and Nonradical Mechanisms, *Environ. Sci. Technol.*, 2018, **52**(15), 8649–8658.

9 G. Huang, C. Wang, C. Yang, P. Guo and H. Yu, Degradation of Bisphenol A by Peroxymonosulfate Catalytically Activated with $Mn_{1.8}Fe_{1.2}O_4$ Nanospheres: Synergism between Mn and Fe, *Environ. Sci. Technol.*, 2017, **51**(21), 12611–12618.

10 P. Sun, H. Liu, M. Feng, Z. Zhai, Y. Fang, X. Zhang, *et al.*, Strategic combination of N-doped graphene and g-C_3N_4: Efficient catalytic peroxymonosulfate-based oxidation of organic pollutants by non-radical-dominated processes, *Appl. Catal., B*, 2020, **272**, 119005.

11 W.-D. Oh, Z. Dong and T.-T. Lim, Generation of sulfate radical through heterogeneous catalysis for organic contaminants removal: Current development, challenges and prospects, *Appl. Catal., B*, 2016, **194**, 169–201.

12 X. Cheng, H. Guo, Y. Zhang, G. V. Korshin and B. Yang, Insights into the mechanism of nonradical reactions of persulfate activated by carbon nanotubes: Activation performance and structure-function relationship, *Water Res.*, 2019, **157**, 406–414.

13 Y. Gao, Y. Zhu, Z. Chen, Q. Zeng and C. Hu, Insights into the difference in metal-free activation of peroxymonosulfate and peroxydisulfate, *Chem. Eng. J.*, 2020, 394.

14 W. Tang, B. Zanli and J. Chen, O/N/P-doped biochar induced to enhance adsorption of sulfonamide with coexisting Cu (2+)/Cr(VI) by air pre-oxidation, *Bioresour. Technol.*, 2021, **341**, 125794.

15 N. Zhao, C. Zhao, D. C. W. Tsang, K. Liu, L. Zhu, W. Zhang, *et al.*, Microscopic mechanism about the selective adsorption of Cr(VI) from salt solution on O-rich and N-rich biochars, *J. Hazard. Mater.*, 2021, **404**, 124162.

16 Z. Wan, Z. Xu, Y. Sun, M. He, D. Hou, X. Cao, *et al.*, Critical Impact of Nitrogen Vacancies in Nonradical Carbocatalysis on Nitrogen-Doped Graphitic Biochar, *Environ. Sci. Technol.*, 2021, **55**(10), 7004–7014.

17 Y. Deng, Phosphorus and kalium co-doped g-C_3N_4 with multiple-locus synergies to degrade atrazine: Insights into the depth analysis of the generation and role of singlet oxygen, *Appl. Catal., B*, 2023, **320**, 121942.

18 X. Li, L. Ye, Z. Ye, S. Xie, Y. Qiu, F. Liao, *et al.*, N, P co-doped core/shell porous carbon as a highly efficient peroxymonosulfate activator for phenol degradation, *Sep. Purif. Technol.*, 2021, **276**, 119286.

19 X. Wang, Biomass derived N-doped biochar as efficient catalyst supports for CO_2 methanation, *J. CO2 Util.*, 2019, **34**, 733–741.

20 Z. Wan, Z. Xu, Y. Sun, M. He, D. Hou, X. Cao, *et al.*, Critical Impact of Nitrogen Vacancies in Nonradical Carbocatalysis on Nitrogen-Doped Graphitic Biochar, *Environ. Sci. Technol.*, 2021, **55**(10), 7004–7014.

21 K. A. Spokas, Review of the stability of biochar in soils: predictability of O:C molar ratios, *Carbon Manage.*, 2010, **1**(2), 289–303.

22 K. Pang, W. Sun, F. Ye, L. Yang, M. Pu, C. Yang, *et al.*, Sulfur-modified chitosan derived N, S-co-doped carbon as a bifunctional material for adsorption and catalytic degradation sulfamethoxazole by persulfate, *J. Hazard. Mater.*, 2022, **424**, 127270.

23 W. Ren, L. Xiong, G. Nie, H. Zhang and S. Wang, Insights into the Electron-Transfer Regime of Peroxydisulfate Activation on Carbon Nanotubes: The Role of Oxygen Functional Groups, *Environ. Sci. Technol.*, 2020, **54**(2), 1267–1275.

24 X. Liu, A Biocha Based Route for Environmentally Friendly Controlled Release of Nitrogen Urea-Loaded Biochar and Bentonite Composite, *Sci. Rep.*, 2019, **9**(1), 9548.